Planta (2019) 249:445–455
https://doi.org/10.1007/s00425-018-3011-x

ORIGINAL ARTICLE

Reconstruction of root systems in *Cryptomeria japonica* using root point coordinates and diameters

Mizue Ohashi[1] · Hidetoshi Ikeno[1] · Kotaro Sekihara[2] · Toko Tanikawa[3] · Masako Dannoura[4,5] · Keitaro Yamase[6] · Chikage Todo[6] · Takahiro Tomita[7] · Yasuhiro Hirano[2]

Received: 24 June 2018 / Accepted: 15 September 2018 / Published online: 20 September 2018

Abstract

Main conclusion **We developed simple algorithms for reconstructing tree root system architecture using only the root point coordinate and diameter, which can be systematically obtained without digging up the root systems.**

Root system architecture (RSA) is strongly related to various root functions of the tree. The aim of this study was to develop a three-dimensional (3D) RSA model using systematically obtained information on root locations and root diameters at the locations. We excavated root systems of *Cryptomeria japonica* and systematically obtained *XYZ* coordinates and root diameters using a 10-cm grid. We clarified the patterns of the root point connections and developed a reconstructed root system model. We found that the root diameters farther from the stump centre are smaller. Additionally, we found that the root lengths of the segments running between the base and the connected root point were smaller than those of other root segments, and the inner angle between the base and the stump and between the base and the connected root point was narrower than for the other pairs. The new RSA model developed according to these results had average accuracies of 0.64 and 0.80 for estimates of total volume and length, respectively. The developed model can estimate 3D RSA using only root point data, which can be obtained without digging up root systems. This suggests a wide applicability of this model in root function evaluation.

Keywords Branching point · Cost function · Diameter · Root model · RSA · *XYZ* coordinates

Introduction

The root system anchors a tree, supporting the aboveground portion by adaptively preventing felling from gale-force winds (Nicoll and Ray 1996). Roots take up soil solution and transport water and nutrient compounds (Pratt et al. 2008) and also affect ions in soil solution (Clarholm et al. 2015).

The root system architecture (RSA) strongly relates to the mechanisms and strengths of root functions. Many studies have described RSA together with functional traits such as the power of mechanical resistance against landslides (e.g. Danjon et al. 2013; Ghestem et al. 2014; Dorval et al. 2016; Liang et al. 2017). The RSA of woody plants is heterogeneous compared to the architecture of the aboveground parts because the soil environment plays a decisive role in root system development (Stokes et al. 1997). Because of the high spatial heterogeneity, full three-dimensional (3D) RSA is preferably obtained using geometry (spatial placements of roots) and topology (connection between individual roots via branching) data of the roots. To measure root geometry

Electronic supplementary material The online version of this article (https://doi.org/10.1007/s00425-018-3011-x) contains supplementary material, which is available to authorized users.

✉ Mizue Ohashi
ohashi@shse.u-hyogo.ac.jp

[1] School of Human Science and Environment, University of Hyogo, Himeji 670-0092, Japan

[2] Graduate School of Environmental Studies, Nagoya University, Nagoya 464-8601, Japan

[3] Kansai Research Center, Forestry and Forest Products Research Institute, Kyoto 612-0855, Japan

[4] Graduate School of Global Environmental Studies, Kyoto University, Kyoto 606-8501, Japan

[5] Graduate School of Agriculture, Kyoto University, Kyoto 606-8502, Japan

[6] Hyogo Prefectural Technology Center for Agriculture, Forestry and Fisheries, Shiso 671-2515, Japan

[7] School of Engineering, University of Hyogo, Himeji 671-2280, Japan

and topology, root structure is often divided into different axes that compose the connection of root branches and the axis is further subdivided into segments (Danjon et al. 1999; Tobin et al. 2007).

Development of a semi-automatic digitizing procedure using multi-scale tree graphs (MTGs) and AMAPmod software enabled us to precisely and rapidly measure the axes and segments and reconstruct the full 3D RSA of uprooted and excavated coarse root systems (Godin et al. 1997; Danjon and Reubens 2008; Sorgonà et al. 2018). The use of a high-resolution laser scanner also offers opportunities to represent 3D RSA (Gärtner et al. 2009). However, excavation of coarse root systems limits the applicability of these techniques. Root excavation is not always feasible because of the inaccessibility of a site, unstable surface soil condition, heavy disturbance of the forest floor, etc.

RSA modelling is a labour-saving technique to reconstruct the full 3D RSA. Formerly, root system modelling was used to evaluate root function, but root data collection for this modelling was often objective dependent and lacked a description of the detailed RSA (e.g. Drexhage and Gruber 1999). However, recent development of RSA models has been useful and holistic, enabling creation of a bridge between evaluation of various functions of the roots (Tobin et al. 2007). RSA models can be categorized into two main types: static models and dynamic developmental models (Tobin et al. 2007). Static models often describe the architecture of existing roots by applying the rules or statistical relationships in the local dimensions observed to whole root systems (e.g. Fitter 1987; Salas et al. 2004). The dynamic growth model is an approach based on the mathematical rules involved in the dynamics of RSA (e.g. Jourdan and Rey 1997). In both the static and growth models, however, it is common that branching points are key information to separate roots into axes or segments (e.g. Namm and Berrill 2016; Ozier-Lafontaine et al. 1999). This means excavation of whole root systems is still required for using these models, which limits the applicability of RSA models.

Ground-penetrating radar (GPR) is a potential tool for collecting the data of the RSA model without digging up the whole roots systems. GPR is a non-destructive geophysical technique, for obtaining root geometry and biometric data much faster and much more easily. Root point is normally determined according to where hyperbolas and higher amplitudes of reflected waves are observed compared to the surrounding area in the radargram. Then, the depth, position, and diameter of the root systems are predicted using the indexes of root points (Butnor et al. 2001; Barton and Montagu 2004; Hirano et al. 2009). However, the weakness of this technique is the difficulty in obtaining root topology data. Since there is no information on the connection between root points in the radargrams, the axes and segments of the roots cannot be established. Recently, Wu et al. (2014) developed an algorithm that estimates the connection of root points on concentric survey lines of GPR and the branching of the root segments. This study showed the possible use of GPR data for representing the 3D RSA.

The final aim of this study was to develop a 3D RSA static model using systematically obtained information on the *XYZ* coordinates and root diameters at the coordinates, not root topology information. In this pursuit, we aimed to (1) clarify the patterns of point connections of roots, which were systematically and manually obtained from an excavated root system; (2) develop an algorithm for reconstructing root systems from data pertaining to the location and diameter of root points; and (3) evaluate the accuracy of the RSA reconstruction model in terms of root connection, volume, length, and biomass by comparing it to estimates using root information obtained from manual measurements. We also evaluated the importance of branching information by comparing the reconstructed models with and without the data at branching points. Finally, we discussed the possible application of GPR data to represent the 3D RSA of mature trees and to evaluate the various functions of forest ecosystems.

Materials and methods

Root excavation

Three root systems of mature *Cryptomeria japonica* were excavated in the experimental forest at the Kansai Research Center, Forestry and Forest Products Research Institute, Kyoto, Japan. *C. japonica* is among the most common species for artificial plantation in Japan, occupying nearly 20% of the entire forested area in Japan. The three root systems were designated Root A, Root B, and Root C. The sampled trees were 27–29 years old and the height and diameter at breast height were 16–18 m and 17–21 cm, respectively. The stems were first cut at approximately 50-cm height, and the ground cover in a ca. 2-m radius surrounding the tree was removed using hand tools prior to the excavation. The upper soil layer was removed manually to expose most of the surface roots. The soil was then loosened to ca. 1 m in depth by repeatedly vertically inserting the shovel of a backhoe into the soil. The whole root systems were then carefully pulled out and excavated using the mechanical shovel of the backhoe. When large roots were broken, the portion left in the soil was dug out with hand tools and attached later to the corresponding location using tape. After harvesting, the attached soil was carefully removed by hand. All fine roots less than 2 mm in diameter and a portion of the small roots 2–5 mm in diameter were removed to analyse root system structure.

Manual measurement

A digital photo of each root system was taken after the harvesting and used later to visually evaluate the accuracy of the 3D RSA modelling. The excavated root systems were then transported to the laboratory of the Kansai Research Center and placed upside down on a sheet with a 10-cm grid.

The *XYZ* coordinates at the root points where roots crossed the 10-cm grid (CPs) were measured manually using a ruler and a plumb bob. The *XYZ* coordinates at the root branching and end points (BPs) were also measured irrespective of the grid. Root diameter at the CPs and BPs, or root point diameter, was measured using a Vernier calliper. Root connections between the measured points were then recorded.

After taking geometric and topologic measurements, the root systems were cut into several pieces. All roots were dried at 70 °C in a drying machine until the weight remained constant and summed to determine the dry weight of the whole root system. Twenty pieces of root 2–5 cm in diameter and ca. 2 cm in length were randomly sampled and their volumes measured using a graduated cylinder. Then, the root density in each piece (gDW m^{-3}) was calculated.

The datasets generated during the current study are available from the corresponding author on reasonable request.

Analysis of root point connections

To identify the rules of connection between the root points, we compared the diameter of the two ends of each root segment determined among the CPs and BPs. Here, we defined the farthest and closest edges to the centre of the stump as P_A and P_B, respectively, and calculated the diameter ratio of the farthest root edge (D_B) to that of the closest edge (D_A) (Fig. 1a). Here, we examined whether D_A is smaller than D_B, i.e. $D_B/D_A > 1$, or not, because roots normally taper toward their apexes (Danjon and Reubens 2008).

We also calculated the length (L_0) and inner angle (θ_0) between the direction from P_A to the centre of the stump and that to P_B for each root segment (Fig. 1b). Thereafter, we identified the other P_Bs (P_{B1}, P_{B2}, …) that share the same P_A and had a larger diameter than that of P_A. The distances (L_1, L_2, …) and the inner angles (θ_1, θ_2, …) were calculated for each pair of P_A and P_B and were compared to the L_0 and θ_0 values of the root segment (Fig. 1b). Then, we created ranking tables of L and θ values for each root segment and determined the rank of L_0 and θ_0 in total in each table. Here, ranking means positioning the L or θ value in the list arranged in order of increasing values. Because the main roots often elongate in a straight manner in a radiating form from the stump (e.g. Wu et al. 2014), we examined whether the length and inner angle of the root segment are shorter and narrower than those of the other pairs of P_A and P_Bs, i.e. rank of L_0 and θ_0 is high.

The cost function for reconstructing the root systems was thereafter established from the characteristics of the length and inner angles of the whole root segments (see "Results").

Modelling and evaluation

We reconstructed the 3D RSA of three *C. japonica* trees using the manual data (RSA_{manual}) and the algorithms of the point connections ($RSA_{modelled}$). They were estimated in two

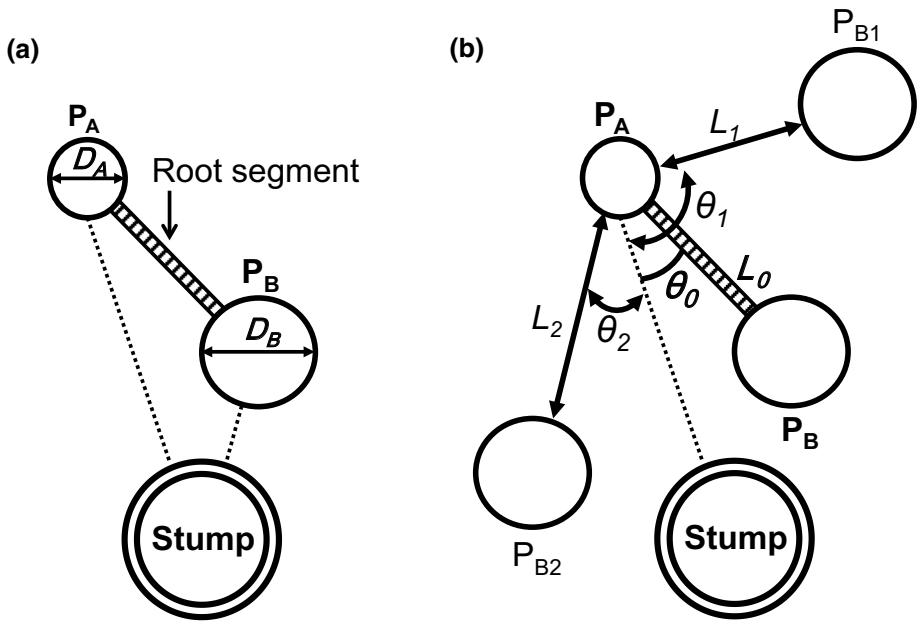

Fig. 1 Diagram of root connection analysis. **a** The diameter ratio of root edges farther from (P_A) and closer (P_B) to the stump (D_B/D_A) was calculated for each root segment. **b** The length (L_0) and inner angle (θ_0) between the direction from the base root point (P_A) to the centre of the stump and that to the connected point (P_B) were calculated. The other PBs that had a larger diameter than that of P_A were searched (P_{B1}, P_{B2}). Then, the lengths (L_1, L_2) and inner angles (θ_1, θ_2) of the pairs of P_A and P_Bs were calculated and compared to the L_0 and θ_0 values, respectively

manners: with branching and end point information (+BP) and without it (−BP).

To reconstruct RSA_{manual}, we used the manual *XYZ* coordinate data and root point diameters and the connecting information between them. Here, we used the data of all root segments among the CPs and BPs for $RSA_{manual}+BP$ and the CPs only for the $RSA_{manual}-BP$.

We estimated $RSA_{modelled}$ using the *XYZ* coordinates and root point diameters. Instead of information on point connection, the algorithms were used. Here, we used the data at the CPs and BPs for $RSA_{modelled}+BP$ and the CPs only for $RSA_{modelled}-BP$.

After the reconstruction of RSA_{manual} and $RSA_{modelled}$, the total root length and volume were calculated for each root system to evaluate the accuracy of the modelling. To calculate the total root length, we assumed that each root segment was straight and summed the lengths of the root segments. We assumed each root segment was a truncated cone and used the length of the segment and the diameters of the two edges to calculate the volume of the root segment. The accuracy of the modelling was then evaluated by dividing the value of $RSA_{modelled}$ by the value of RSA_{manual}. Total root biomass of RSA_{manual} was calculated by multiplying the total root volume with average root density and compared to the value of the original root system (Table 1). We also compared the root connection between $RSA_{manual}+BP$ and $RSA_{modelled}+BP$, and between $RSA_{manual}-BP$ and $RSA_{modelled}-BP$.

Results

Belowground properties of mature *C. japonica* trees

On average, the total number of point coordinates in each root system of *C. japonica* was 599. It was more than 650 in Root A and Root C, but only 460 in Root B (Table 1). Branching and end points occupied 20%, 18%, and 19% of the total points of Root A, Root B, and Root C, respectively. The whole dry weight of the root system including the stump was 19.2 kg on average and was the largest in Root A and the smallest in Root B (Table 1). Root density was 440 ± 85 kg m^{-3} on average.

Table 1 Aboveground and belowground properties of the three *C. japonica* trees

	Root A	Root B	Root C
Age (year)	27	29	28
Height (m)	16.7	17.8	18.1
Stem diameter at breast height (cm)	21.0	17.2	19.5
Number of all point coordinates	686	458	654
Points crossing with the 10 cm grid, CP	552	376	531
Branching and end points, BP	134	82	123
Total root weight (kg)	25.4	11.3	21.0
Stump (kg)	11.0	4.9	7.7
Coarse roots > 5 mm in diameter (kg)	14.4	6.4	13.3

Root point diameter was distributed similarly among the three root systems (Fig. 2a). The average diameters ranged from 15.5 to 16.3 mm. They concentrated within a range of 5–10 mm and the percentage of root points that had a diameter less than 10 mm was nearly 55% in all root systems (Fig. 2a). The maximal, minimal, and average distances from the root point to the stump were 125–162, 10–17, and 57–72 cm, respectively (Fig. 2b). They were distributed similarly in Root A and Root C, with an arch-like shape, but not in Root B. In Root B, more than 80% of the root points were located within 75 cm of the stump (Fig. 2), showing an aggregated distribution surrounding the stump compared to the other two stumps.

Patterns of point connections

We found that more than 77% of the root diameter ratios of the root segments (D_B/D_A) were > 1.0 in all three root systems (Fig. 3). Of these, 59–69% of the ratio ranged from 1 to 2, showing that the root segments were slightly thicker toward the stump.

The length of root segment (L) was mostly between 25 and 125 mm in all three root systems (Fig. 4a). Here, 79–83% of the L values fell within this range. The frequency distributions of the inner angle (θ) between the direction from the farthest edges of the root segment to the stump and that to the closest edges were biased to lower values in the tree roots (Fig. 4b). Here, 24–28% of the θ values were within the range of 0°–10° and 44–49% within the range of 0°–20°. This shows that many of the root segments towards the stump had a sharp inner angle.

A comparison of root segments to the other pairs of point connections that share the same root point farther from the stump showed that the length of the root segment was shorter than those of the other pairs of point connections (Fig. 5a). The length of 53–58% of the root segments was the shortest in all the pairs of root point connections that shared the same farther root points (Fig. 1b) and 70–73% of the root segments were the second shortest (Fig. 5). Moreover, 96–98% of the root segments ranked in the top ten. The root inner angle between the direction from the farther point to the stump and that to the closer point (Fig. 1b) was also smaller than those of the other pairs sharing the same farther point in many root segments, but lower ranks were also observed (Fig. 5b). Moreover, 29–38% of the root segments were ranked in the top 10 and 44–58% of the root segments were ranked in the top 20.

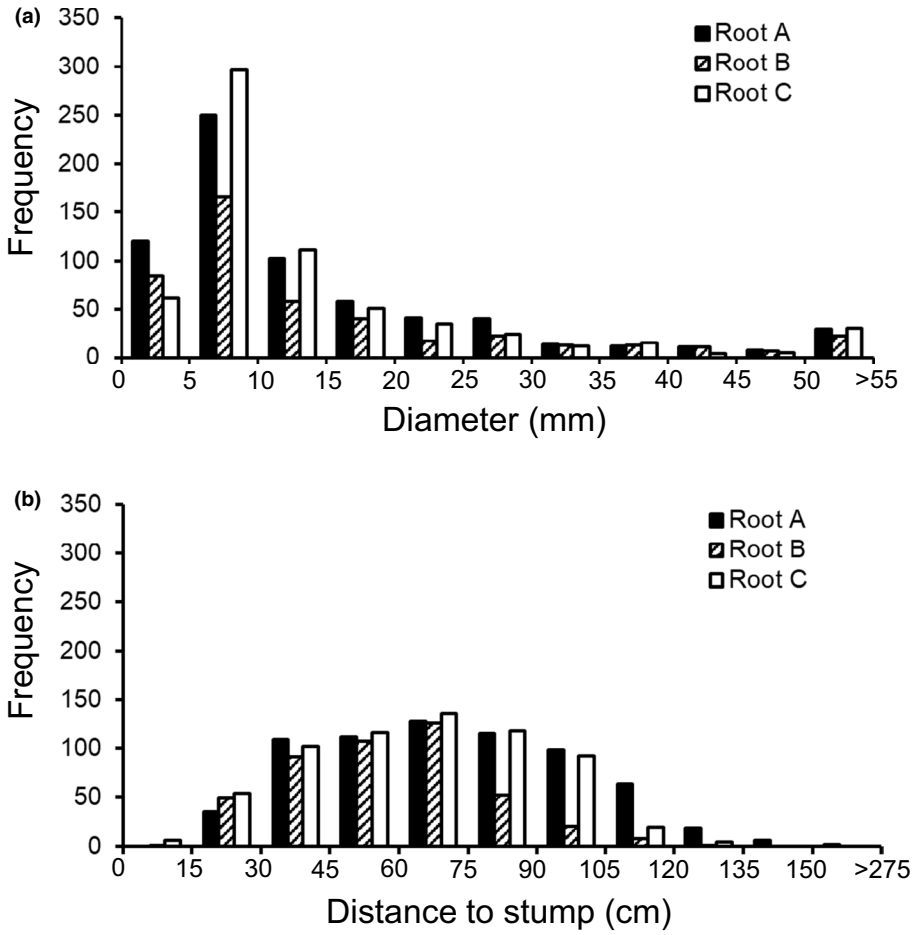

Fig. 2 Frequency distribution of root point diameter using a 5-mm interval (**a**) and distance to the centre of stump using a 15-cm interval (**b**) at the root point. Root point means the location where the roots crossed the 10-cm grid (CPs) and branching and end points (BPs)

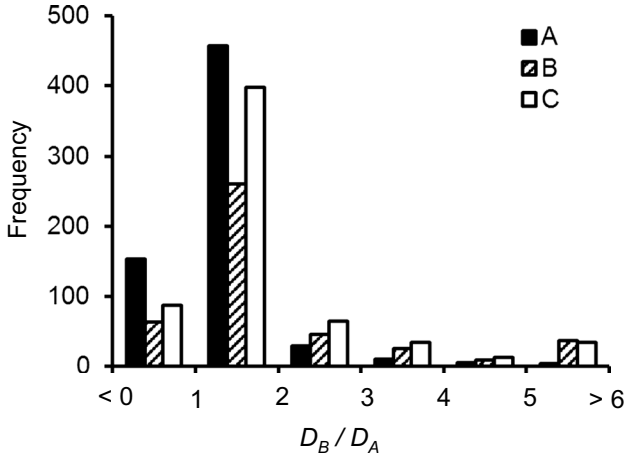

Fig. 3 Frequency distribution of D_B/D_A of root segment with one interval. *D* is the diameter at the edges of the root segment. A and B are the farther and closer edges of the root segment from the stump centre

Model establishment

In this study, we established models for reconstructing the 3D RSA of *C. japonica* trees with the following conditions (Fig. S1):

1. Selection of a target root point: start from the farthest point from the stump.
2. Comparison of root diameter to other root points: select larger diameters for candidates to connect.
3. Conducting calculations and selection of the connecting point: for every candidate point, cost function values are calculated and the point with the minimal cost is selected as the connecting point.

The cost function was formulated by combining the distance between the target root point and a candidate root point (*L*) and the normalized scalar product of the two vectors, one from the target point to the centre of stem and the other to the connecting point (cosθ) (Fig. 1b). Here, we assumed the following two conditions in the cost function formula, which were derived from the pattern of the point connections of the three root systems:

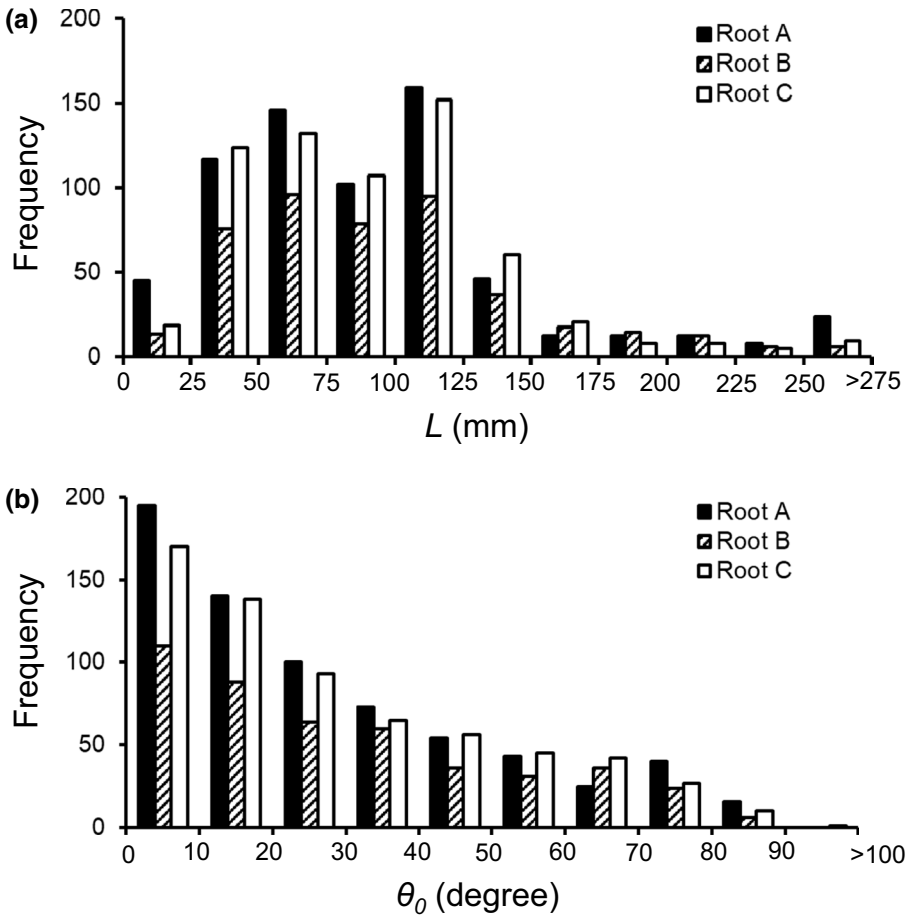

Fig. 4 Frequency distribution of the length using a 25-cm interval (**a**) and an inner angle between the direction from the base root point (P_A) to the centre of the stump and that to the connected point (P_B) were calculated (θ_0) using a 30° interval (**b**). Here, P_A and P_B are the edges of the root segment farther from and closer to the stump, and both the CPs and BPs are included

1. The distance between the base point and connected point (L_0) is smaller than in the case of the other pairs (L_1, L_2, …).
2. The inner angle between the direction from the base point to the centre of the stump and to the connected point (θ_0) is smaller than those of the other points (θ_1, θ_2, …).

Then, the cost function was formulated and the values were calculated for every candidate point as follows:

$$F(\theta, L) = (1 - \cos(\theta)) + w \cdot L/L_{\max}, \quad (1)$$

where L is the distance, θ is the angle, w is the weight parameter, and L_{max} is the maximal length between two root points. In this equation, direction and distance factors were considered normalized by setting one to a maximal value. The source code of our modelling program can be downloaded from GitHub, https://github.com/HidetoshiIkeno/RootReconstruct.

Model evaluation

We found that the accuracy of the reconstruction varied depending on the weight parameter, w (Fig. 6). Therefore, we adjusted the best w value for each data set (+BP or −BP) of each root system (Root A, Root B, or Root C). The best w values of Root A, Root B, and Root C were 0.06, 0.07, and 0.06 for an RSA with branching information (+BP) and 0.09, 0.23, and 0.12 for an RSA without branching information (−BP), respectively.

The 3D RSA reconstructed from the manual data including branching information (RSA_{manual} + BP) showed similarity to the photo of the original root system (Fig. 7). The estimates of the root biomass of RSA_{manual} + BP were 20.2, 11.8, and 18.5 kg for Root A, Root B, and Root C, respectively, 40–85% greater than those of the original roots (Table 1).

The top and side views of the 3D RSA reconstructed from the point connection algorithms ($RSA_{modelled}$) showed a very

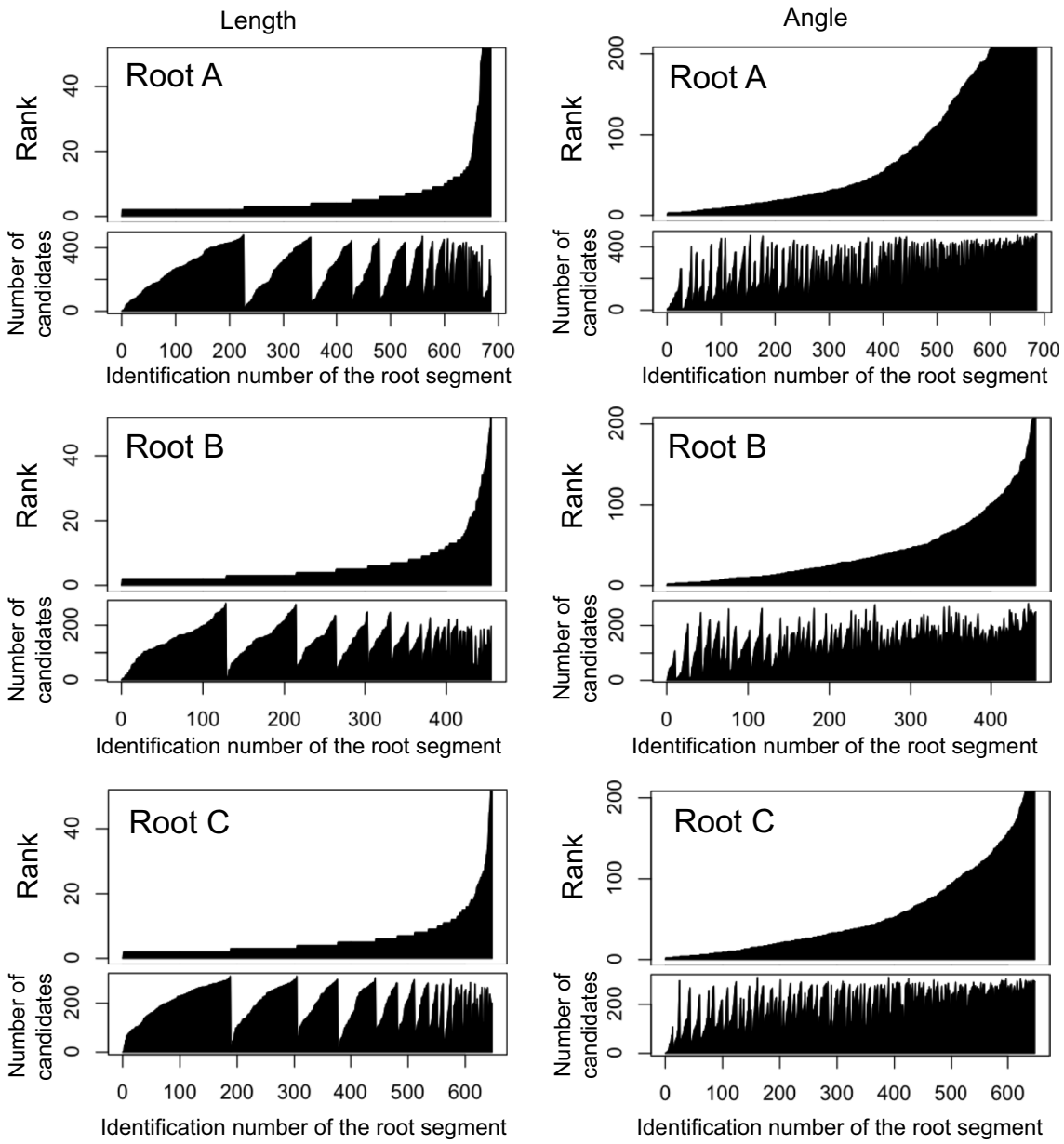

Fig. 5 The rank of the root segment in the pairs of root point connections that share the same base point with the root segment. The black bar indicates the ranks of the root segments in ascending order. Grey bars indicate the number of point connections for each root segment. The root points that had a larger diameter were connected to the base point and the length (L) and angle (θ) between them were compared to those of the root segment. See also Fig. 1b for a detailed explanation of point selection. For length, 96–98% of the root segments ranked in the top ten. For angles, 44–58% of the root segments were in the top 20

similar overview to those using manual data (RSA_{manual}) irrespective of the inclusion of branching information (+BP) or not (−BP) (Figs. S2 and S3). The modelling accuracies for total volume and length were always 0.90 and 0.87 on average, respectively, when compared between $RSA_{modelled}$ and RSA_{manual} (Table 2). However, the accuracy of the point connections was lower than those of volume and length, 0.68 on average with branching information, and 0.59 on average without branching information (Table 2).

When we compare $RSA_{modelled} - BP$ to $RSA_{manual} + BP$, the accuracies for total volume and length were 0.64 and 0.80 on average, respectively. They were particularly high in Root A, 0.76 and 0.91 for volume and length, respectively. On the other hand, the accuracy for the total volume of Root C was the lowest at just 0.43.

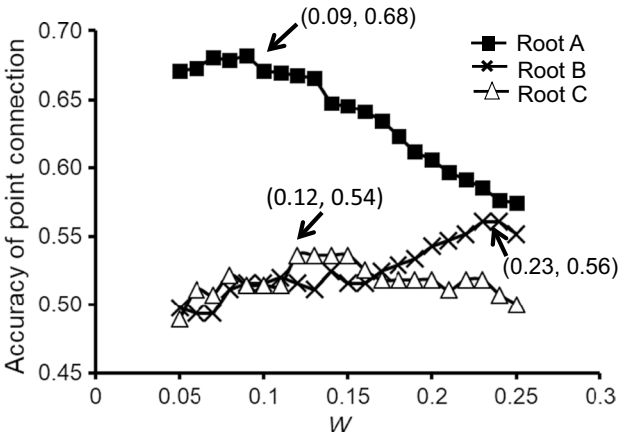

Fig. 6 Relationship between w value and accuracy of the point connection of $RSA_{model}-BP$. The w values at their highest accuracy are shown for each root system in the graph

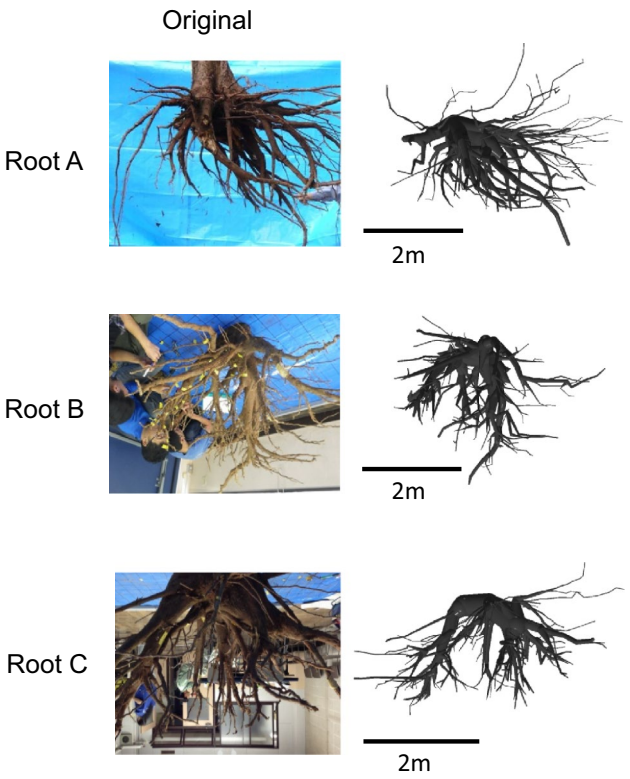

Fig. 7 Comparison of 3D RSA in the photo of the original tree and the drawing from the manual data. Roots in the originals were cut out and then rotated and reversed to be aligned in the direction of 3D RSA from the manual data

Discussion

In this study, we succeeded in developing a 3D RSA static model using only the information on the *XYZ* coordinates and root point diameters. Our RSA model can predict the RSA of mature *C. japonica* trees with an accuracy > 0.54, even though the dataset does not include the branching information of the root systems. When we include the branching information, the accuracy of the estimates of total volume and length were > 0.78 and that of point connection > 0.65. These results show that the 3D RSA of *C. japonica* trees can be approximately estimated from simple geometric and topologic data. Our results also suggest that branching information is not essential to estimate the RSA of a tree. Many of the previous RSA models, including both of the static and dynamic types, require the information of branching points to reconstruct RSA. Therefore, excavation of root systems and searching branching points are almost unavoidable. Although the *XYZ* coordinates of root points can be measured automatically using 3D low-magnetic-field digitizing devices (Danjon et al. 1999) and/or 3D laser beam devices (Gärtner et al. 2009), it is complicated and time-consuming work. Also, the length of the root segment is determined to most accurately describe the structure in previous studies (Tobin et al. 2007; Danjon et al. 1999). In our model, on the other hand, the length of root segments is defined as the shortest distance between the root locations. This means our model has a strong advantage, namely, systematic measurements of root geometry and topology using grids or circular lines can be conducted, which is a simpler and quicker approach for collecting data for 3D RSA reconstruction.

Our model suggests the possible application of GPR data to represent the 3D RSA of mature trees. GPR can predict the depth, position, and diameter of root systems without digging up the roots (Butnor et al. 2001; Cui et al. 2013; Tanikawa et al. 2013, 2016; Guo et al. 2015). Previous studies have shown that GPR can detect roots in soil with less than 30% volumetric water content where sufficient relative dielectric permittivity contrast can be generated between the roots and the surrounding soil (Cui et al. 2013). Therefore, a number of studies have used GPR for root detection in various soil types thus far (Hirano et al. 2012; Guo et al. 2013, 2015; Wu et al. 2014; Borden et al. 2017), suggesting wide applicability of the technique to obtain root geometry information in soil. Zenone et al. (2008) suggested a possible use of GPR to map entire root systems by comparing the results of GPR scans and the point clouds obtained via laser scanning of the root system after its excavation. Hruška et al. (1999) attempted to redraw 3D views of *Quercus petraea* root systems manually from the GPR radargram and confirmed its accuracy by removing the soil. Recently, Wu et al. (2014) succeeded in estimating the root point connection of the shrubby tree *Caragana microphylla* using GPR. In these techniques, roots points of GPR need to be collected on neighbouring concentric survey lines. On the other hand,

Table 2 Accuracy of total volume, length and point connection of modelled RSA evaluated by comparing with the estimates of RSA from manual data

	With branching and ending points (+BP)			With branching and ending points (−BP)			Accuracy (4)/(1)
	RSA_{manual} (1)	$RSA_{modelled}$ (2)	Accuracy (2)/(1)	RSA_{manual} (3)	$RSA_{modelled}$ (4)	Accuracy (4)/(3)	
Total volume (m^3)							
Root A	0.046	0.036	0.78	0.039	0.035	0.90	0.76
Root B	0.027	0.024	0.89	0.020	0.020	1.00	0.74
Root C	0.042	0.042	0.98	0.021	0.018	0.87	0.43
Average	0.038	0.034	0.88	0.027	0.024	0.92	0.64
Total length (m)							
Root A	68	55	0.95	58	51	0.89	0.91
Root B	44	40	0.92	40	32	0.82	0.77
Root C	59	55	0.93	58	42	0.72	0.71
Average	53	50	0.94	52	42	0.81	0.80
Point connection							
Root A			0.66			0.68	
Root B			0.65			0.56	
Root C			0.72			0.54	
Average			0.68			0.59	

the reconstruction model of our study estimates point connections irrespective of the shapes of survey lines. It requires only information on *XYZ* coordinates and the diameter at multiple root points.

However, since GPR has a limited ability to estimate root diameter, the accuracy of modelling might change depending on the ability of GPR. In general, high-frequency GPR has a high resolution, but fails to obtain root points at deep depths (Guo et al. 2013). Our data showed most of the diameters at the root points were less than 15 mm (Fig. 2a). Since Hirano et al. (2009) reported that the diameter of the smallest detectable root was 19 mm for a 900 MHz GPR system, it might be difficult to detect the roots using this antenna frequency. Guo et al. (2013) summarized the root diameter estimation by radar techniques, which showed roots with 0.5 mm diameter in 30 cm depth were detected using 1500 MHz GPR. Since root distribution normally concentrates on the soil surface layer, 1500 MHz GPR might be enough to detect the root systems. Combination of high and low antennae frequency would be another option to detect roots in both surface and deep layers. The detection of roots varies not only by antenna frequency, but also by many other factors such as soil water content and adjacent root distribution (Dannoura et al. 2008, Yamase et al. 2018). Therefore, we should carefully select the antennae frequency suitable for detecting the target root systems. In this study, if we exclude the root point data with < 10 mm diameter, the average accuracy of $RSA_{modelled}-BP$ drops from 0.64 to 0.50. This suggests that overlooking of small roots by GPR would give minor impacts on volume estimates, but the impact would change depending on the purposes of RSA reconstruction. Further studies should combine the 3D RSA reconstruction model in this study with the root data obtained by GPR techniques.

In this study, the accuracy of the RSA model decreased significantly for Root C when BP point information was excluded (Table 2). This might mean there was an insufficient number of the CPs for Root C, causing an increase in the relative importance of the BPs. To utilize the developed model, we need to investigate how the number of root point data necessary for each purpose is decided.

Our results showed that the weight parameter, w, was higher in $RSA_{modelled}-BP$ than that in $RSA_{modelled}+BP$ (Figs. S2 and S3) The w value controls the balance of the inner angle (θ) and length (L) between root points when the connected root point is selected. If w increases, it means that the model places more emphasis on the length data for the selection of the connected point. Therefore, the increase in the w value in the models without branching information means that the importance of length increases when the branching information is removed. In this study, the comparison of the root segment to the other pairs of point connections that share the same point with the root segment showed that the root length was highly ranked compared to the root angle (Fig. 5). For length, more than 70% of the root segments were in the top two, but for inner angle, only 29–38% of the root segments were in the top ten. However, our model assumes that both the length and inner angle of the root segment are the smallest in the pairs of point connections. This creates more connection mistakes with increasing emphasis on inner angles. The increase in the best w value in $RSA_{modelled}-BP$ means the information on BPs was important to use for the angle data.

Our results also showed the best *w* value changed in the three root systems. This means we need to clarify the changes in the *w* value patterns and the factors controlling them. Our results also suggest that *w* values are almost same if the information of branching point is included (0.06–0.07, Figs. S2 and S3). Though the branching point data were excluded, the accuracy of point connection with the changes in *w* value does not vary much in Root B and C (Fig. 6). Only in Root A, change of *w* value seriously affects the accuracy of point connection (Fig. 6). In our model, increase of *w* value means length information is more important for predicting the RSA. Therefore, the decrease of accuracy with the increase of *w* value might be caused by the large curvedness of the coarse root systems as we can sees in the picture of original Root A (Fig. 7). Additional information is necessary for identifying the manner of how to choose the best *w* value. Changes in *w* values among tree species, age, and size of root systems should be examined.

Conclusion

In this study, we showed the patterns of point connections of *C. japonica* roots, in which the root points were systematically and manually obtained. These findings allowed us to develop simple algorithms for reconstructing RSA using only the *XYZ* coordinates and root point diameters, which can be obtained by GPR techniques without digging up the root systems. The reconstructed RSA showed high accuracy in estimating root volume and length, suggesting the applicability of this model to evaluate root functions. However, RSA has high plasticity, changing size and form drastically with variation in tree species and soil environments. Because we analysed only the RSAs of *C. japonica* growing in the same experimental forest, additional studies of various RSAs are necessary to broaden the usage of this model across different species and sites.

Author contribution statement KS and YH conceived and designed the research. KS, TT, MD, KY, CT and YH conducted the experiments. MO and HI analysed the data. TT and HI developed the model. MO and HI wrote the manuscript. All authors read and approved the manuscript.

Acknowledgements We appreciate H. Hagino, T. Chikaguchi, S. Narayama, H. Kurokawa, Y. Yamamoto (FFPRI), K. Okada, M. Takano (Nagoya Univ.), M. Hiraoka (Tokyo Univ. Agr. Tech.), Y. Shinohara (Kyushu Univ.), N. Makita, K. Tsuruta, and J. Tsuruta (Kyoto Univ.) for their field assistance and valuable comments on this study. This work was partially supported by the Japanese Society for the Promotion of Science KAKENHI (Grant numbers: 25252027, 18H02243).

Compliance with ethical standards

Conflict of interest All the authors declare that they have no conflict of interest.

References

Barton CVM, Montagu KD (2004) Detection of tree roots and determination of root diameters by ground penetrating radar under optimal condition. Tree Physiol 24:1323–1331

Borden KA, Thomas SC, Isaac ME (2017) Interspecific variation of tree root architecture in a temperate agroforestry system characterized using ground-penetrating radar. Plant Soil 410:323–334

Butnor JR, Doolittle JA, Kress L, Cohen S, Johnsen KH (2001) Use of ground-penetrating radar to study tree roots in the Southeastern United States. Tree Physiol 21:1269–1278

Clarholm M, Skyllberg U, Rosling A (2015) Organic acid induced release of nutrients from metal-stabilized soil organic matter—the unbutton model. Soil Biol Biochem 84:168–176

Cui X, Guo L, Chen J, Chen X, Zhu X (2013) Estimating tree-root biomass in different depths using ground-penetrating radar: evidence from a controlled experiment. IEEE Trans Geosci Remote Sens 51:3410–3423

Danjon F, Reubens B (2008) Assessing and analyzing 3D architecture of woody root systems, a review of methods and applications in tree and soil stability, resource acquisition and allocation. Plant Soil 303:1–34

Danjon F, Sinoquet H, Godin C, Colin F, Drexhage M (1999) Characterisation of structural tree root architecture using 3D digitising and AMAPmod software. Plant Soil 211:241–258

Danjon F, Khuder H, Stokes A (2013) Deep phenotyping of coarse root architecture in *R. pseudoacacia* reveals that tree root system plasticity is confined within its architectural model. PLoS One 8:e83548. https://doi.org/10.1371/journal.pone.0083548

Dannoura M, Hirano Y, Igarashi T, Ishii M, Aono K, Yamase K, Kanazawa Y (2008) Detection of *Cryptomeria japonica* roots with ground penetrating radar. Plant Biosyst 142:375–380

Dorval AD, Meredieu C, Danjon F (2016) Anchorage failure of young trees in sandy soils is prevented by a rigid central part of the root system with various designs. Ann Bot 118:747–762

Drexhage M, Gruber F (1999) Above- and below-stump relationships for *Picea abies*: estimating root system biomass from breast-height diameters. Scand J For Res 14:328–333

Fitter AH (1987) An architectural approach to the comparative ecology of plant-root systems. New Phytol 106:61–77

Gärtner H, Wagner B, Heinrich I, Denier C (2009) 3D laser scanning—a new methodology to analyze coarse tree root systems. For Snow Landsc Res 82:95–106

Ghestem M, Veylon G, Bernard A, Vanel Q, Stokes A (2014) Influence of plant root system morphology and architectural traits on soil shear resistance. Plant Soil 377:43–61

Godin C, Costes E, Caraglio Y (1997) Exploring plant topological structure with the AMAPmod software: an outline. Silva Fenn 31:355–366

Guo L, Chen J, Cui X, Fan B, Lin H (2013) Application of ground penetrating radar for coarse root detection and quantification: a review. Plant Soil 362:1–23

Guo L, Wu Y, Chen J, Hirano Y, Tanikawa T, Li W, Cui X (2015) Calibrating the impact of root orientation on root quantification using ground-penetrating radar. Plant Soil 395:289–305

Hirano Y, Dannoura M, Aono K, Igarashi T, Ishii M, Yamase K, Makita N, Kanazawa Y (2009) Limiting factor in the detection of tree roots using ground-penetrating radar. Plant Soil 319:15–24

Hirano Y, Yamamoto R, Dannoura M, Aono K, Igarashi T, Ishii M, Yamase K, Makita N, Kanazawa Y (2012) Detection frequency of *Pinus thunbergii* roots by ground penetrating radar is related to root biomass. Plant Soil 360:363–373

Hruška J, Cermak J, Sustek S (1999) Mapping tree root systems with ground penetrating radar. Tree Physiol 19:125–130

Jourdan C, Rey H (1997) Modelling and simulation of the architecture and development of the oil-palm (*Elaeis guineensis* Jarq) root system-1. The model. Plant Soil 190:217–233

Liang T, Knappett JA, Bengough AG, Ke YX (2017) Small-scale modelling of plant root systems using 3D printing, with applications to investigate the role of vegetation on earthquake-induced landslides. Landslides 14:1747–1765

Namm BH, Berrill J-P (2016) Tanoak (*Notholithocarpus densiflorus*) coarse root morphology: prediction models for volume and biomass of individual roots. Open J For 6:1–13

Nicoll BC, Ray D (1996) Adaptive growth of tree root systems in response to wind action and site conditions. Tree Physiol 16:899–904

Ozier-Lafontaine H, Lecompte F, Sillon JF (1999) Fractal analysis of the root architecture of *Gliricidia sepium* for the spatial prediction of root branching, size, and mass. Model development and evaluation in agroforestry. Plant Soil 209:167–180

Pratt RB, Jacobsen AL, North GB, Sack L, Schenk HJ (2008) Plant hydraulics: new discoveries in the pipeline. New Phytol 179:590–593

Salas E, Ozier-Lafontaine H, Nygren P (2004) A fractal model applied for estimating root biomass and architecture in two tropical legume tree species. Ann For Sci 61:337–345

Sorgonà A, Proto AR, Abenavoli LM, Di Iorio A (2018) Spatial distribution of coarse root biomass and carbon in a high-density olive orchard: effects of mechanical harvesting methods. Trees. https://doi.org/10.1007/s00468-018-1686-z

Stokes A, Nicoll BC, Coutts MP, Fitter AH (1997) Responses of young Sitka spruce clones to mechanical perturbation and nutrition: effects on biomass allocation, root development and resistance to bending. Can J For Res 27:1049–1057

Tanikawa T, Hirano Y, Dannoura M, Yamase K, Aono K, Ishii M, Igarashi T, Ikeno H, Kanazawa Y (2013) Root orientation can affect detection accuracy of ground-penetrating radar. Plant Soil 373:317–327

Tanikawa T, Ikeno H, Dannoura M, Yamase K, Aono K, Hirano Y (2016) Leaf litter thickness, but not plant species, can affect root detection by ground penetrating radar. Plant Soil 408:271–283

Tobin B, Čermák J, Chiatante D, Danjon F, Di Iorio A, Dupuy L, Eshel A, Jourdan C, Kalliokoski LR, Nadezhdina N, Nicoll B, Pagès L, Silva J, Spanos I (2007) Towards developmental modeling of tree root systems. Plant Biosyst 141:481–501

Wu Y, Guo L, Cui XH, Chen J, Cao X, Lin H (2014) Ground-penetrating radar-based automatic reconstruction of three-dimensional coarse root system architecture. Plant Soil 383:155–172

Yamase K, Tanikawa T, Dannoura M, Ohashi M, Todo C, Ikeno H, Aono K, Hirano Y (2018) Ground penetrating radar estimates of tree root diameter and distribution under field conditions. Trees. https://doi.org/10.1007/s00468-018-1741-9

Zenone T, Morelli G, Teobaldelli M, Fischanger F, Matteucci M, Sordini M, Armani A, Ferre C, Chiti T, Seufert G (2008) Preliminary use of ground-penetrating radar and electrical resistivity tomography to study tree roots in pine forests and poplar plantations. Funct Plant Biol 35:1047–1058